Moliner Marin, M.; Gabay, JE.; Kliewer, CE.; Carr, RT.; Guzman, J.; Casty, GL.; Serna Merino, PM.... (2016). Reversible Transformation of Pt Nanoparticles into Single Atoms inside High-Silica Chabazite Zeolite. Journal of the American Chemical Society. 138(48):15743-15750. doi:10.1021/jacs.6b10169

Reversible transformation of Pt nanoparticles into single atoms inside high-silica CHA

Manuel Moliner,[a] Jadeene E. Gabay,[b] Chris E. Kliewer,[c] Robert T. Carr,[c] Javier Guzman,[d] Gary L. Casty,[c] Pedro Serna,[c]* Avelino Corma[a]*

[a] Instituto de Tecnología Química, Universitat Politècnica de València-Consejo Superior de Investigaciones Científicas, Avenida de los Naranjos s/n, 46022 Valencia, Spain

[b] Astrix Technology Group, 125 Half Mile Road, Suite 200, Red Bank, New Jersey 07701, United States

[c] ExxonMobil Research and Engineering Co., Annandale, New Jersey 08801, United States

[d] ExxonMobil Chemical Company , 4500 Bayway Drive Baytown, Baytown, Texas 77520, United States

ABSTRACT: We report the encapsulation of platinum species in highly siliceous chabazite crystallized in the presence of N,N,N-trimethyl-1-adamantammonium and a thiol-stabilized Pt complex. When compared to Pt/SiO_2 or Pt-containing Al-rich zeolites, the materials in this work show enhanced stability towards metal sintering in a variety of industrial conditions, including H_2, O_2 and H_2O. Detailed structural determinations by XAS and AC HAADF-STEM demonstrate subtle control of the supported metal structures from ~ 1 nm nanoparticles to single Pt atoms, via reversible interconversion of one species into another in reducing and oxidizing atmospheres. The combined used of microscopy and spectroscopy is critical to understand these surface-mediated transformations. When tested in hydrogenation reactions, Pt/CHA converts ethylene (~80%) but not propylene under identical conditions, in contrast to Pt/SiO_2, which reacts both at similar rates. These differences are attributed to the negligible diffusivity of propylene through the small pore zeolite, and provide a final evidence of the metal encapsulation.

1.- Introduction

Transition metals on solid supports are ubiquitous industrial catalysts for the synthesis of many chemicals.[1,2] Typically, high dispersion is desirable for better utilization of the precious metal, and most dispersed sites (i.e. clusters and single atoms) often facilitate unique catalysis that is not achieved by conventional bulk-like structures.[3,4] Unfortunately, metals tend to sinter over time in reactive environments leading to reduction in catalyst lifetime by loss of available metal surface area, and/or by the annihilation of those unique metal ensembles. The concept of sinter resistant supports has been proposed and taken on a number of incarnations, including strong bonding between the support and the metal,[5,6] and various strategies to capture metals in support cavities.[7-9] When the support is a well-structured microporous solid, such as a zeolite, opportunities for encapsulation of the metal nanoparticles in their channels arise.[10] A number of metal-containing zeolites, particularly those with medium (~5-5.5 Å) and large pores (~6.5-7 Å), have been prepared via post-synthetic methodologies such as metal impregnation or cation exchange.[11-13] These zeolites offer high-surface areas to disperse the metal effectively, yet their relatively large pores do not confine the smallest nanoparticles and prevent their aggregation under severe reaction conditions.[14]

Trapping metals within small pore zeolites have recently received attention to enhance the sinter-resistance of metals.[15] Traditional post-synthetic approaches show limitations to incorporate the metal in small pore zeolites, in particular with metal cations of large ionic radii. One-pot methods have been proposed and must be developed to circumvent this synthetic challenge.[16,17]

Transition metal nanoparticles have been encapsulated within different low-silica small-pore zeolites, such as LTA,[14,16,18-22] RHO,[23] or GIS.[24] These materials are prepared without organic structure directing agent (OSDA) at very low crystallization temperatures (~80-100°C); thus, only limited zeolites with very Al-rich frameworks (Si/Al ratio < 3) has been achieved. While these results are interesting, low silica zeolites suffer from low hydrothermal stability and weaker acidity than Si-rich materials, which limits their applications as catalysts. As such, the synthesis of metal nanoparticles encapsulated in high-silica small pore zeolites would be of both fundamental and practical interest.

Zeolites with high Si/Al ratios are synthesized using OSDA molecules,[25] often at high crystallization temperatures (above 150°C) and high pH. In these conditions, most metal precursors tend to precipitate as rather large bulk metal hydroxides when added to the synthesis media.[16] Earlier literature demonstrates that thiol compounds stabilize metal nanoparticles, which can be dispersed in an

amorphous high-surface silica matrix using a one-pot synthetic approach.[26] The high thermal stability of these mercapto-based organometallic complexes has been also demonstrated under alkaline hydrothermal conditions.[17]

Among the different small pore zeolites reported in the literature, CHA, formed by a three-directional small pore system containing large cavities,[27] is an attractive candidate considering its diversity in chemical compositions,[15,27-29] crystal sizes (20 nm to 3 μm),[30] and catalytic applications.[31,32]

Herein, we present the direct synthesis of a nanocrystalline (20-50 nm) high-silica CHA zeolite containing encapsulated Pt nanoparticles of ~1 nm, using the combination of N,N,N-trimethyl-1-adamantammonium (TMAda) and Pt-mercapto complex as OSDA and Pt-precursor, respectively. These Pt nanoparticles have remarkable stability; they maintain ~1 nm size at 650°C in H_2 and steam. Moreover, quantitative transient Extended X-Ray Absorption Fine Structure (EXAFS) demonstrate that ~1 nm Pt nanoparticles fragment into site-isolated single Pt atoms in O_2 as the temperature increases from 100 to 500°C. Particles then re-form at 80-150°C in H_2, leading to a fully reversible cluster formation/fragmentation cycle that enables fine tuning of the catalytic structures from single metal atoms to ~1 nm. *In situ* X-Ray Absorption Spectroscopy (XAS) and aberration-corrected High-Angle Annular Dark-Field Scanning Transmission Electron Microscopy (AC HAADF-STEM) are used to investigate dynamic changes in the metal structures during the thermal treatments. The combination of both "average" (spectroscopy) and "local" (microscopy) information is shown critical to properly understand these surface-mediated transformations.

Table 1. Synthesis conditions selected for the Pt-containing high-silica CHA materials (Si/Al=15, TMAda/Si=0.2, H_2O/Si=20, the resultant gels have been treated at T= 90°C for 7 days, and later, at 160°C for 2 or 7 days under dynamic conditions).

Sample	NaOH/Si	Pt/Si [%wtPt]	TMSH/Pt
Pt-CHA-1	0.4	0.00033 [0.11]	3
Pt-CHA-2	0.4	0.00033 [0.11]	15
Pt-CHA-3	0.2	0.00033 [0.11]	15
Pt-CHA-4	0.4	0.001 [0.33]	15

2.- Experimental

2.1.- Synthesis of metal-containing zeolites

2.1.1.- Synthesis of N,N,N-trimethyl-1-adamantammonium

29.6 g of 1-Adamantamine (Sigma-Aldrich) and 64 g of potassium carbonate (Sigma-Aldrich) were mixed with 320 ml of chloroform. At this point, 75 g of methyl iodide was added dropwise while the reaction was stirred in an ice bath. The reaction was maintained during 5 days under agitation at room temperature. The mixture was filtered and washed with diethyl ether, and the resultant solid further extracted with chloroform. The final product was N,N,N-trimethyl-1-adamantammonium iodide. This iodide salt was anion exchanged using an ion exchange resin achieving the hydroxide form.

2.1.2.- Synthesis of Pt-containing high-silica CHA materials

The synthesis conditions for the synthesis of the Pt-containing CHA materials are summarized in Table 1. The procedure followed to carry out the preparation of the Pt-containing high-silica CHA materials is exemplified for the particular synthesis of the Pt-CHA-2 material. In this case, 800 mg of sodium hydroxide (99%, Sigma-Aldrich) was dissolved in 6.9 g of water. Then, 86 mg of a 10%wt aqueous solution of chloroplatinic acid ($H_2PtCl_6.6H_2O$, 37.50% Pt basis, Sigma-Aldrich) and 52 mg of (3-mercaptopropyl)trimethoxysilane (TMSH, 95%, Sigma-Aldrich) were added to the above solution, and the mixture stirred for 30 minutes. Afterwards, 13.04 g of an aqueous solution of N,N,N-trimethyl-1-adamantammonium hydroxide (TMAdA, 16.2%wt) was added and maintained under stirring during 15 minutes. At that time, 293 mg of aluminum hydroxide (66%wt, Sigma-Aldrich) was added, and the resultant mixture kept under stirring at 80ºC for 30 minutes. Finally, 3 g of colloidal silica (Ludox AS40, 40%wt, Aldrich) was introduced in the synthesis mixture, and maintained under stirring at 80ºC for 30 minutes. The final gel composition was SiO_2 : 0.033 Al_2O_3 : 0.00033 Pt : 0.005 TMSH : 0.2 TMAdA : 0.4 NaOH : 20 H_2O.

The gel was transferred to an autoclave with a Teflon liner, and heated at 90°C for 7 days, and later, at 160°C for 2 days under dynamic conditions. The sample after the hydrothermal crystallization was filtered and washed with abundant distilled water, and finally dried at 100°C.

2.1.3.- Synthesis of aluminum-rich Pt-LTA material (Pt-LTA)

A Pt-containing Al-rich LTA material has been synthesized following the methodology described by Iglesia et al.,[17] under the following synthesis conditions.

SiO2 : 0.7 Al_2O_3 : 0.002 Pt : 0.06 TMSH : 2.2 NaOH : 60 H_2O; T=100°C.

The gel was transferred to an autoclave with a Teflon liner, and heated at 100°C for 2 days under dynamic conditions. The sample after the hydrothermal crystallization was filtered and washed with abundant distilled water, and finally dried at 100°C. After the synthesis procedure, the obtained solid shows the crystalline structure of the LTA material.

2.1.4.- Synthesis of Pt/SiO_2

A catalyst consisting of platinum nanoparticles supported on amorphous silica (reference material) was prepared according to the process described in the literature.[33] In this procedure, 1.784 g of tetraammine platinum hydroxide was mixed with 12.2 g of deionized water. 0.6 g of arginine was added to this solution so that the arginine to Pt molar ratio was 8:1. The solution was added by incipient wetness onto 10.0 g of Davison silica (grade 62, 60-200 mesh, 150 Angstrom pore diameter from Sigma-Aldrich).

The sample was dried at 120°C for 2 hrs. The dried sample was placed in a tube furnace with an active air flow of 300 sccm of air, with the heating rates being maintained at 3 °C/min to 400°C and then maintaining the temperature at 400°C for 16 hrs. The chemical analysis of the resultant solid by ICE-AES indicated a Pt content of 0.8 %wt.

2.2.- Characterization

Powder X-ray diffraction (PXRD)

PXRD measurements were performed with a multisample Philips X'Pert diffractometer equipped with a graphite monochromator, operating at 45 kV and 40 mA, and using Cu K_α radiation (λ = 0.1542 nm).

Chemical analyses

The chemical analyses were carried out in a Varian 715-ES ICP-Optical Emission spectrometer, after solid dissolution in HNO_3/HCl/HF aqueous solution.

Electron microscopy

The morphology of the samples was studied by scanning electron microscopy (SEM) using a JEOL JSM-6300 microscope and by scanning transmission electron microscopy (STEM) using a JEM 2100F microscope.

H_2 chemisorption

Metal dispersions in the calcined samples have been determined by H_2 chemisorption at 313 K using the double isotherm method on a Quantachrome Autosorb-1 equipment after *in-situ* reduction of the sample at 673 K for 2 h under pure hydrogen flow, assuming a H:Pt adsorption stoichiometry of 1:1.

XAFS Experiments

XAFS experiments were performed at beamline 9-BN at Advanced Photon Source (APS) at the Argonne National Laboratory. Data were collected in fluorescence mode using a XAFS cell that also acted as a flow reactor. The samples were scanned in the presence of flowing gases (30 sccm) at variable temperatures. 4 % H2 (in He) was used to perform the in situ reductions, whereas 20 % O2 (in He) was used for the in situ oxidation treatments.

The storage ring electron energy and ring currents were 7.0 GeV and 105 mA, respectively. A water-cooled Si(111) monochromator was used to scan X-ray energy from -250 to 1000 eV relative to Pt L3 edge (11564 eV). Each sample (~20 mg) was pressed as a thin wafer inside an air tight EXAFS cell, using a multi-ion Ge detector to collect data in fluorescence mode. Transmission XAFS measurements were carried out simultaneously with the pure Pt metals measured in reference mode for X-ray energy calibration and data alignment. Data processing and analysis were performed using the IFEFFIT package.[34] EXAFS analysis was done model-independently, and the results were not biased in favor of any assumed model about the short-range order of elements in these samples. Specifically, multiple-edge (Pt L3) analysis was employed by fitting theoretical FEFF6 calculations [35] to the experimental EXAFS data in *r* space. The values of passive electron reduction factor, S_0^2, were obtained to be 0.80 by fits to their corresponding standards, and were fixed in the analysis of the Pt-CHA samples. The parameters describing electronic properties (e.g., correction to the photoelectron energy origin) and local structural environment (coordination numbers *N*, bond length *R*, and their mean-squared relative derivation, σ^2) around absorbing atoms were varied during fitting. In addition, the physically reasonable constraints between the fitting parameters for the first nearest neighbor (1NN) pairs were applied.

Structure of active sites by aberration-corrected HAADF-STEM

All environmental and high resolution imaging studies were conducted using a JEOL 2200FS AC STEM/TEM FEG operated at 200 kV. The microscope's probe forming system was fitted with a CEOS GmBH hexapole corrector. Simultaneous bright field (BF) and high angle annular dark field (HAADF) STEM images were acquired as 512 x 512 px scans at 64 ms/px using Gatan's Digital MicrographTM software. Metal particle size data was measured from the digital images using Gatan's Digital MicrographTM software. Particle size data was plotted using KaleidaGraphTM software. Environmental studies were conducted in the JEOL 2200FS STEM mode using a Protochips Atmosphere In-Situ Gas Cell System utilizing MEMS heating technology. All reactions were conducted at 1 Torr under either 5% H2 / 95% Ar or 100% O2.

2.3.- Catalytic test

In a typical experiment, 40 mg of the Pt-CHA-2 (0.21 wt % Pt) or 10 mg of the Pt/SiO_2 (0.8 wt % Pt) catalysts were mixed with 1 g of neutral silica (silica gel, Davisil Grade 640, 35- 60 mesh) and loaded in a conventional tubular plug-flow reactor (ID = 6/16 inches 9.53 mm). High purity hydrogen, ethylene, propylene, and nitrogen were used for the experiments, with flow rates regulated by standard mass flow controllers. The temperature of the catalyst bed was controlled using a three-zone vertical furnace (ATS, model 3210) with a precision of ± 1°C. Prior to the hydrogenation experiment, the catalyst was reduced in situ in flow of hydrogen (50 sccm) at 400°C for 4 h. The reactor was then cooled down to the selected reaction temperature (80°C). With the catalyst bed at 80 ± 1 °C, the reaction mixture was flowed at atmospheric pressure: 4 sccm of alkene (ethylene or propylene); 20 sccm of H_2; and 100 sccm of N_2. The downstream reaction effluents were analyzed in a gas chromatograph (Agilent 5975B) connected in series, and equipped with a 50 m capillary column (Rt-Alumina BOND/Na_2SO_4, 0.53 mm ID, 10 μm) and a FID detector. The conditions of the analysis were: initial oven temperature = 50 °C; temperature ramp = 10 °C/min; final oven temperature = 180 °C; injector temperature = 220 °C; detector temperature = 320 °C; pressure at the head of the column = 9.7 psi. For identification purposes, the position of the various reactants and products within the gas chromatogram were compared with standards commercially available. Conversions and selectivity were calculated from the corresponding GC areas.

3.- Results and discussion

3.1.-Synthesis and stability of Pt-containing high-silica CHA zeolite

To accomplish efficient encapsulation of Pt inside high-silica CHA, we investigated different synthesis parameters such as NaOH/Si [0.2, 0.4], TMSH/Pt [5, 15], and Pt content [0.11 and 0.33%wt Pt] (Table 1). Other variables where chosen according to typical conditions to obtain metal-free CHA.[27,36]

Table 2. Chemical analyses on Pt-containing high-silica CHA materials.

Sample	Si/Al	%wtPt
Pt-CHA-1	7.8	0.23
Pt-CHA-2	8.5	0.21
Pt-CHA-3	12.2	0.17
Pt-CHA-4	8.0	0.45

The powder X-ray diffraction patterns (PXRD) of the resultant solids indicate the formation of pure CHA in all studied cases (Figure 1). The Pt-CHA-3 sample, synthesized with a NaOH/Si ratio of 0.2, required 7 days to crystallize and yielded crystals of ~300 nm (Figure S1), as opposed to samples prepared at a higher NaOH/Si ratio (0.4), which fully crystallized after 2 days and formed 20-40 nm particles (Figure 1 and S2). Changes in the synthesis pH also caused changes in the solid yields, and in the molar Si/Al ratios, both lower when the pH was higher (Table 2) likely due to a fast nucleation of the silico-aluminate and a partial dissolution of the silica phase in the aqueous media under very alkaline conditions.[37] Nonetheless, the Si/Al ratios (> 8.5) are much higher than any other reported for noble metals in small pore zeolites.[16,18,23]

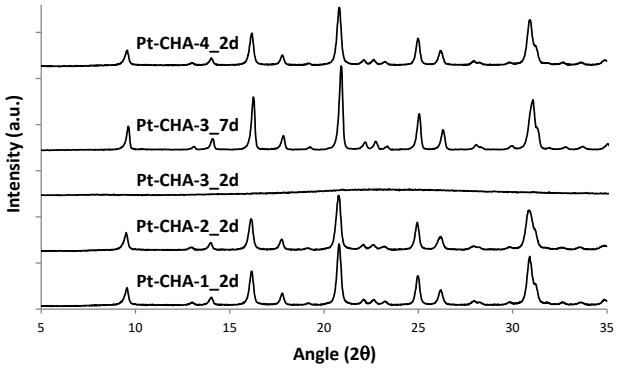

Figure 1. PXRD patterns of the as-prepared materials.

The Pt content in the samples above ranges between 0.2-0.45%wt, depending on the nominal amounts in the synthesis gel (Tables 1 and 2). The dispersion of the metal phase was investigated by STEM after calcination of the materials in air at 580°C, and after subsequent reduction in H_2 at 400°C. The Pt-CHA-2 sample showed the smallest and narrowest distribution of Pt particles (Figure 2), with an average particle size of ~1.4 nm (Figure 3) that is in good agreement with H_2 chemisorption data (~1.7 nm, Table 3). This result drastically contrasts that observed for Pt-CHA-3, synthesized at a lower pH, where a major fraction of the metal is in particles > 20 nm (Figure 2). We hypothesize that poor mobilization of the zeolite precursors at lower pH caused an inefficient encapsulation in Pt-CHA-3.

Small metal nanoparticles were found in materials synthesized at high pH, as in Pt-CHA-2, but using lower TMSH/Pt ratios (Pt-CHA-1, 5 vs 15), or higher Pt contents (Pt-CHA-4, 0.45 vs 0.21 %wt), yet together with Pt aggregates > 20 nm (Figure 2). Thus, we infer that optimal results are achieved when high pH, low metal loading, and high thiol-to-platinum are used (Pt-CHA-2).

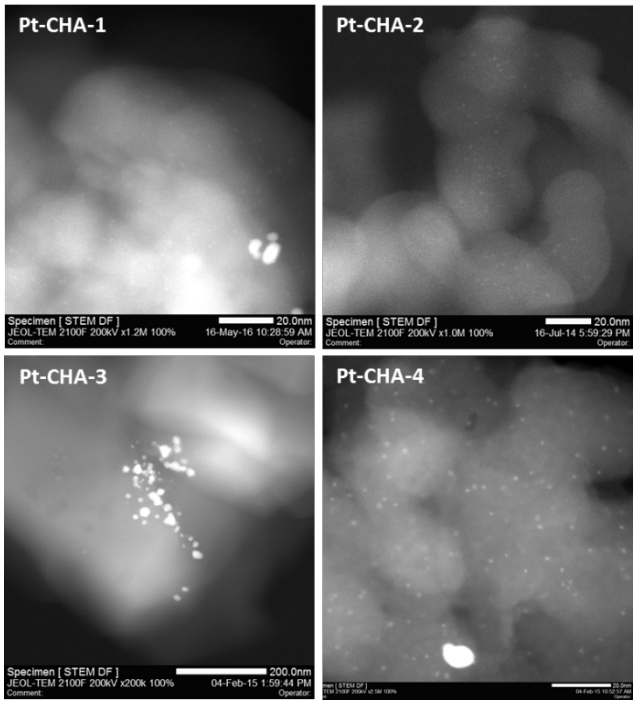

Figure 2. STEM images for the calcined Pt-containing high-silica CHA after being treated with H_2 at 400°C.

Table 3. Pt dispersion and Pt average particle size measured by H2 chemisorption for the Pt-CHA-2 and Pt- SiO2 after different redox treatments.

Sample	Treatment	% dispersion Pt	Average size (nm)
Pt-CHA-2	R400	68.0	1.7
	O650/R400	63.0	1.8
Pt-SiO_2	R400	53.0	2.1
	O650/R400	1.5	7.1

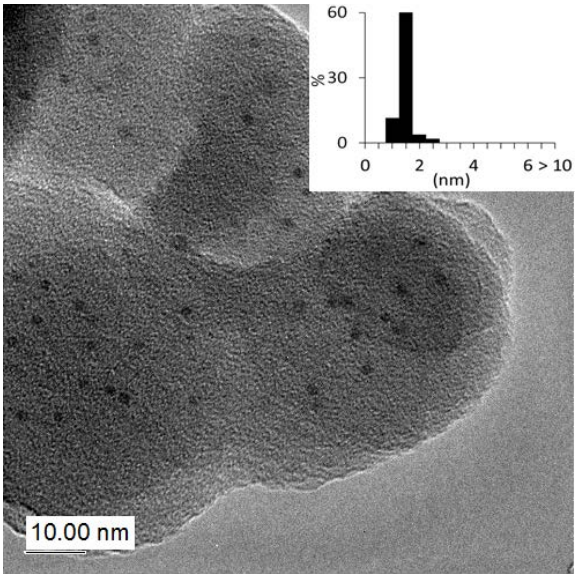

Figure 3. TEM and corresponding Pt nanoparticle size distribution histogram for sample Pt-CHA-2 after reduction in H_2 at 400°C.

The stability of Pt-CHA-2 was then evaluated after high temperature oxidation/reduction treatments, to emulate conditions used to regenerate metal catalysts industrially (i.e. O_2 to remove coke deposits in hydrocarbon transformations, and H_2 to re-activate the metal function). STEM and H2 chemisorption (Figure S3 and Table 3) demonstrate that the Pt-CHA-2 sample retains ~1.3 nm particles after a $H_2/O_2/H_2$ cycle at 400/650/400°C for 2/4/2h, respectively. In contrast, treatment of non-encapsulated Pt nanoparticles, supported on amorphous SiO_2, under analogous conditions resulted in massive sintering of the metal phase; particles grew from ~2 to ~15 nm, on average (Table 3). Remarkably, Pt-CHA-2 retained structural characteristics (i.e. Pt ~1.4 nm) even at harsher conditions ($H_2/O_2/H_2$ at 650/650/650ºC for 6h per step).

We also treated the Pt-CHA-2 material with steam at high temperatures, because vapor water is common in many industrial streams and is often responsible for hydrothermal degradation of the metal and/or the zeolite framework. After subjecting Pt-CHA-2 to a severe steaming process (600°C for 4h), no evidence of the formation of large Pt particles was observed, and the zeolite crystallinity was retained (Figures S4 and S5). In contrast, the zeolitic structure in Pt-containing Al-rich small pore zeolites, prepared according to literature,[17] collapsed under equivalent conditions, resulting in the formation of large Pt particles (e.g. Pt-LTA in Figures S4 and S5).

3.2.- Structure of CHA-Encapsulated Platinum Species in Reducing and Oxidizing Atmospheres

We used XAS spectroscopy to gain more detailed structural information on the Pt-CHA-2 sample (Figures S6 and 4). Fitting of the EXAFS data indicate the presence of ~4 S atoms bonded to a single Pt atom in the as-made material, with a Pt–S distance of 2.32 Å (Table 4, Entry 1). This is consistent with Pt-thiol complexes in square planar coordination formed by reactions of the mercaptosilane and $PtCl_6^{2-}$.[17] Calcination in air at 550°C resulted in complete sulfur removal, and the formation of ~3 Pt–O bonds at 2.01 Å (Table 4, Entry 2). EXAFS does not provide evidence of Pt–Pt bonds in either the as-made or calcined materials, consistent with the absence of Pt nanoparticles visible in STEM micrographs (Figure S2). We conclude that the calcined material consists of isolated PtO_3 units inside the zeolite. Similar species have been reported on KLTL zeolite upon calcination of $[Pt(NH_3)_4](NO_3)_2$ at moderate temperatures (250°C), with the support acting as a macroligand that provides two O-atoms to anchor the Pt.[38]

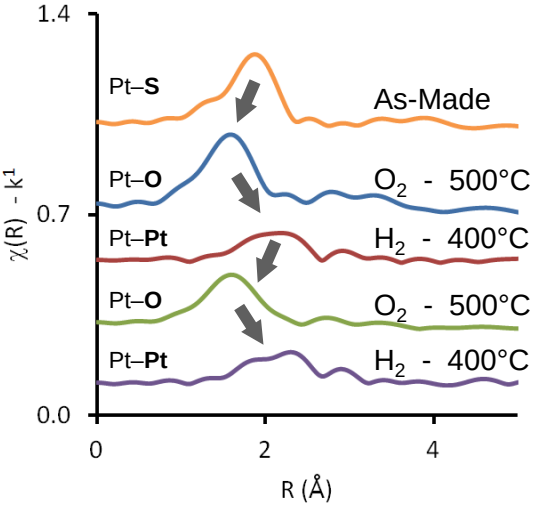

Figure 4. FT-EXAFS spectra of Pt-CHA-2 after various thermal treatments (the arrows indicate direction of the sequence and corresponding changes in structural features) First O_2 treatment performed in an oven in air (removal of organic components). Following treatments performed in a flow EXAFS cell under 30 sccm of 4 % H_2 or 20 % O_2.

Subsequent contact with H_2 at increasing temperatures caused gradual reduction of the metal in Pt-CHA-2, as evidenced by a gradual decrease of the white line intensity in time-resolved XANES experiments (Figure 5A). Well-defined isosbestic points along the treatment suggest a rather simple stoichiometric transformation of one species into another.[39] Eventually, a steady white line intensity equal to that of a Pt foil is reached, indicating full reduction of all the metal in the sample. Figure 5B shows the degree of metal reduction at each temperature, with 0% reduction assigned to the sample before introducing H_2, when the white line intensity is highest, and 100% reduction assigned to the catalyst at the end of the treatment, when it is lowest. The data indicates that the onset temperature for reduction is <100°C, and that full reduction is virtually accomplished at ~150°C. With the metal fully reduced in H_2 at 400°C, EXAFS indicates the presence of a single contribution ascribed to Pt–Pt bonds at 2.74 Å, with an average

Pt-Pt coordination number of ~7 (Table 4, Entry 3), consistent with particles of ~1.5 nm,[40] and thus, consistent with our STEM results (Figure 2).

Table 4. EXAFS data at the Pt LIII edge characterizing the Pt-CHA-2 sample after various thermal treatments.[a]

Entry	Contribution	N	R (Å)	$\Delta\sigma^2$ (Å^2)	ΔE_0 (eV)
1[b]	Pt-S	3.78	2.33	0.0039	7.71
2[c]	Pt-O	3.22	2.01	0.0016	12.4
3[d]	Pt-Pt	7.36	2.74	0.0580	5.83
4[e]	Pt-O	2.71	2.02	0.0034	8.36
5[f]	Pt-Pt	6.48	2.73	0.0071	5.34
	Pt-O	0.44	2.11	0.0011	11.87

[a] Notation: N, coordination number; R, distance between absorber and backscatterer atoms; $\Delta\sigma^2$, Debye–Waller factor; ΔE_0, inner potential correction. Error bounds (accuracies) characterizing the structural parameters obtained by EXAFS spectroscopy are estimated to be as follows: coordination number N, ~20%; distance R, ~0.02; Debye– Waller factor $\Delta\sigma^2$, ~20%; and inner potential correction ΔE_0, ~20%.
[b] Sample as-made; spectra taken in He at 25°C.
[c] Sample in Entry 1 after *ex situ* calcination in air at 550°C for 2 h; spectra taken in air at 25°C.
[d] Sample in Entry 2 after subsequent *in situ* reduction in 4 % H_2 (balance, He) at 400°C for 1h; spectra taken in H_2 at 25°C
[e] Sample in Entry 3 after subsequent *in situ* calcination in 20 % O_2 (balance, He) at 500°C for 1h; spectra taken in air at 25°C
[f] Sample in Entry 4 after subsequent *in situ* reduction in 4 % H_2 (balance, He) at 500°C for 1h; spectra taken in air at 25°C

We then recorded XANES spectra during a subsequent treatment in O_2 as the temperature was raised from temperature 20°C to 500°C. Figure 5C shows gradual increase of the white line intensity, corresponding to oxidation of the metal species. Again, well-defined isosbestic points are observed. Figure 5D, showing the degree of oxidation at various temperatures (based on the white line intensities), reveals that the conversion process takes place continually in the entire temperature range investigated. Steady state was only achieved at the highest temperature (500°C). At this point, EXAFS show the lack of Pt-Pt interactions, and the re-appearance of a Pt-O contribution with a Pt–O bonding distance of 2.01 Å and a Pt–O coordination number of ~3 (Table 4, Entry 4). Redispersion of the platinum nanoparticles in O_2 at 500°C to single Pt atoms could be confirmed using AC HAADF-STEM (Figure S7). Remarkably, the cluster formation process could be reversed upon subsequent reduction of the sample in H_2 at 400°C, with the formation of new ~1.2 nm Pt particles as demonstrated by both EXAFS (Pt-Pt coordination number ~6, Table 4, Entry 5), and STEM (Figure S3).

The materials reported above allow precise reversible transformation of single Pt atoms and ~1 nm nanoparticles depending on the chemical environment and thermal conditions employed. Such a fine, cyclic control of metal species on supports is unusual, and often requires mild temperatures to avoid irreversible formation of large metal aggregates upon sintering. Rh and Ir, for example, made under inert conditions from well-define organometallic compounds such as $Rh(C_2H_4)_2(acac)$ and $Ir(C_2H_4)_2(acac)$ — acac is acetylacetonate — allow reversible transformation between small metal clusters (2-6 atoms) and single-atom metal complexes in H_2 and C_2H_4 atmospheres, respectively, at temperatures below 80°C.[41,42] Single Pt atoms, on the other hand, could be synthesized in a large pore zeolite (KLTL) exchanged with $[Pt(NH_3)_4](NO_3)_2$ and calcined at 250°C.[38] This framework allows stabilization of small Pt nanoparticles (~1-1.5 nm) in H_2 provided that the temperature is < 510°C.[43] Here, by using the further constrained pore system of CHA zeolite, small Pt nanoparticles (~1-1.5 nm) and single Pt atoms could be stabilized in H_2 and O_2, respectively, at temperatures as high as 650°C, and we

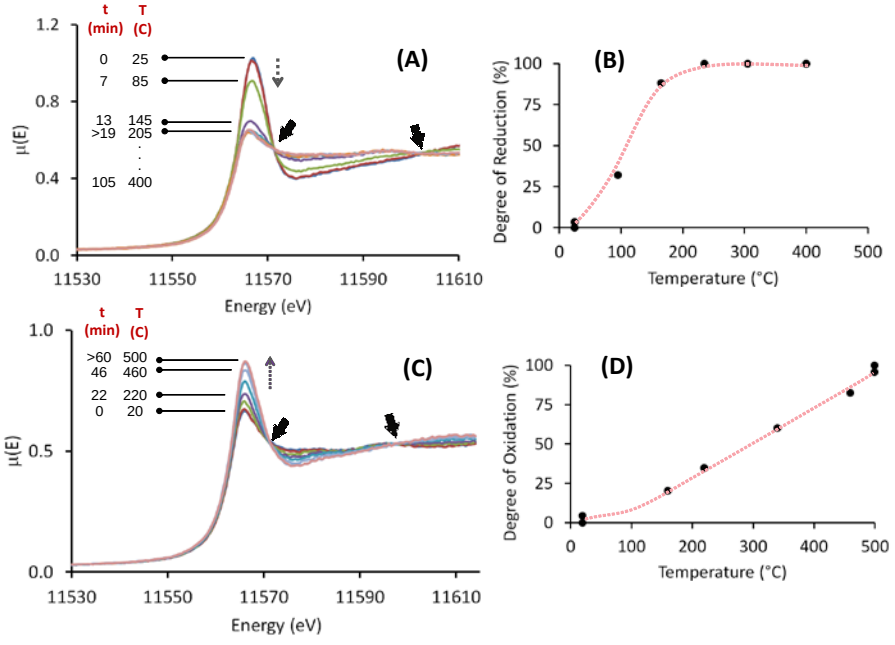

Figure 5. (A) Time-resolved XANES spectra of Pt-CHA-2 (previously calcined in air at 500°C) in 4 % H_2 as the temperature is ramped from 25°C to 400°C at 10°C /min; (C) Time-resolved XANES spectra of Pt-CHA-2 (previous reduced in H_2 at 400°C) in 20 % O2 as the temperature is ramped from 25°C to 500°C at 10°C /min; (B) and (C) show the degree of reduction and oxidation, respectively, as a function of the temperature, according to white intensities (details in main text). The solid arrows point the formation of well-defined isosbestic points during the treatments.

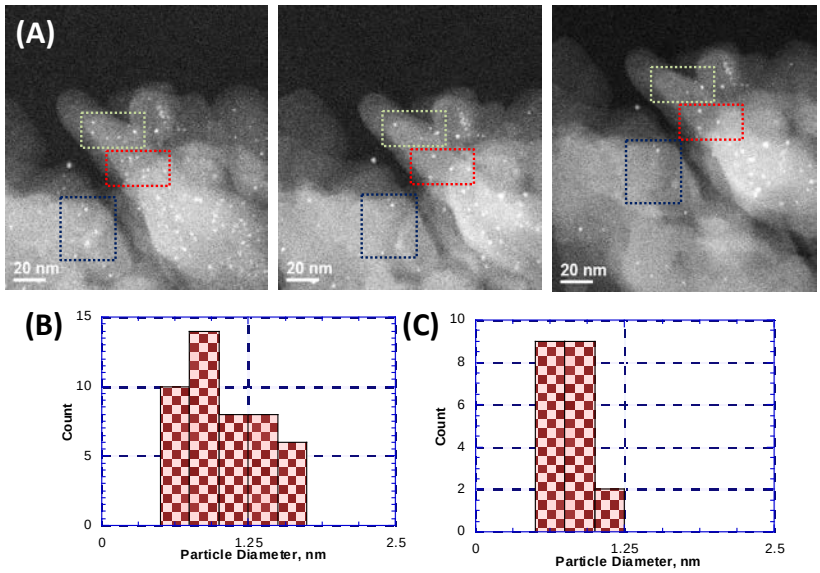

Figure 6. (A) Aberration corrected HAADF-STEM images after contacting the reduced Pt-CHA-2 catalyst with O_2 at 500ºC for increasing times inside an environmental STEM cell (left, 0 min; middle, 10 min; right, 20 min) The areas highlighted show gradual disappearance of particles over time; (B) particle size distribution of Pt-CHA-2 of the reduced Pt-CHA-2 (left); and (C) fraction of particle that disappear during the 20 min in situ O_2 treatment in the TEM cell (the biggest particles remain).

demonstrate that these species can be reversibly interconverted.

3.3.- Oxidative fragmentation of platinum nanoparticles to single platinum atoms inside CHA

To provide better understanding of the cluster breakup process, structural determinations by EXAFS at intermediate calcination temperatures (100 and 200°C) were performed, starting from a fully reduced Pt-CHA-2. Figure S8 and Table 5 show these EXAFS data together with the spectra of the material prior to introduction of O_2 (fully reduced), and after calcination at 500°C (fully oxidized). The results evidence a gradual decrease of the Pt-Pt contribution in O2, from ~7 to ~5, ~4, and ~0 at 100, 200, and 500°C, respectively (Table 5 and Figure S9). These changes were accompanied by gradual increase of the Pt-O coordination number from ~0 to ~1.1, ~1.6, and ~3 at 100, 200, and 500°C, respectively (Table 5 and Figure S9). Based on this information, a decrease in the average particle size can be insinuated,[40] corresponding to ~1.3, ~1.0, ~0.80, and ~0.35 nm (diameter of a single platinum atom) at 25°C, 100, 200, 500°C, respectively.

However, EXAFS provides average structural information and is therefore insufficient to picture some details of the cluster fragmentation process.[44] Thus, we used in-situ AC HAADF-STEM to gather local structural information. After exposure of the reduced Pt-CHA-2 material to O_2 at 500°C inside the microscopy cell, gradual disappearance of the initial Pt nanoparticles is observed (Figure 6). Some particles remained apparently intact even at long contact times and we infer that the treatment inside the TEM cell is less efficient than that in an ideal flow reactor, where complete fragmentation of the metal particles was observed (*vide supra*). The experiment, nonetheless, reveals that the smallest Pt clusters (0.8-1 nm) are more prone to fragmentation than particles in the 1-1.5 nm size range (Figure 6C). Thus, we propose that breakup of the smallest platinum clusters at low temperature is responsible for the initial decay of the Pt-Pt coordination number during our EXAFS experiments (Table 5), with disintegration of increasingly larger crystallites as the severity of the oxidation treatment is increased.

Table 5. EXAFS data at the Pt LIII edge characterizing the reduced Pt-CHA-2 sample upon oxidation at various temperatures.[a]

Gas	T (°C)	Contribution	N	R (Å)	$\Delta\sigma^2$ (Å^2)	ΔE_o (eV)
4% H_2[b]	25	Pt-Pt	7.36	2.74	0.0580	5.83
20% O_2[c]	100	Pt-Pt	5.06	2.72	0.0087	6.84
	100	Pt-O	1.13	2.00	0.0039	5.48
20% O_2[c]	200	Pt-Pt	4.01	2.71	0.010	7.28
	200	Pt-O	1.62	1.99	0.0039	5.37
20% O_2[c]	500	Pt-Pt	-	-	-	-
		Pt-O	2.71	2.02	0.0035	8.36

[a] Notation: *N*, coordination number; *R*, distance between absorber and backscatterer atoms; $\Delta\sigma^2$, Debye–Waller factor; ΔE_o, inner potential correction. Error bounds (accuracies) characterizing the structural parameters obtained by EXAFS spectroscopy are estimated to be as follows: coordination number N, ~20%; distance *R*, ~0.02; Debye– Waller factor $\Delta\sigma^2$, ~20%; and inner potential correction ΔE_o, ~20%.

[b] Measured after reduction of the sample in 4 % H2 at 400°C for 1h; spectra collected at 25°C in H_2.

[c] Measured upon attainment of a steady white line intensity in the XANES spectra (typically, after 1h min in the 20 % O2 stream); spectra collected at 25°C in O_2.

3.4.- Catalytic activity of the CHA-encapsulated Pt nanoparticles

Finally, we used the hydrogenation of olefins of different sizes to demonstrate the successful encapsulation of Pt within the CHA structure. We selected ethylene (0.39 Å) and propylene (0.45 Å), because at mild temperatures the

former diffuses relatively fast through the zeolite, whereas the latter diffuses very slowly.[45] As shown in Figure 7, the Pt-CHA-2 catalyst converts > 80% of ethylene (to ethane) and only 2% of propylene (to propane) under identical experimental conditions. In drastic contrast, a Pt/SiO_2 sample consisting of 2 nm (average) Pt nanoparticles produces similar conversion of both olefins under the same reaction conditions (Figure 7), as one would expect in the absence of internal diffusion effects. The very low catalytic activity observed for the propylene using Pt-CHA-2 unambiguously confirms the effective encapsulation of the Pt nanoparticles within cavities of the high-silica CHA material.

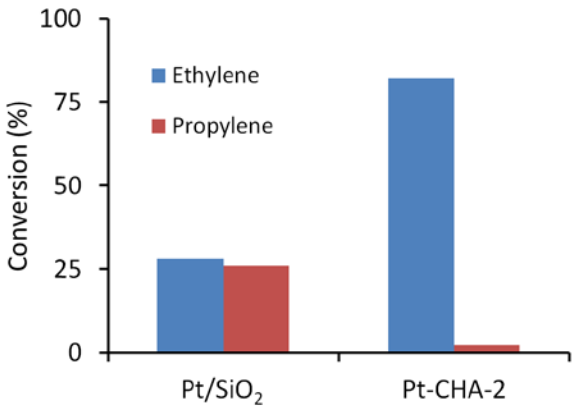

Figure 7. Hydrogenation of ethylene and propylene using 0.2 wt % Pt-CHA-2 (40 mg) and 0.8 wt % Pt/SiO2 (10 mg) as catalysts. Reaction feed: H_2 (20 sccm), alkene (4 sccm); and N_2 (100 sccm). Reaction temperature: 80°C. Catalyst were reduced in H_2 at 400ºC prior to reaction.

4.- Conclusions

In summary, we have demonstrated the direct synthesis of nanocrystalline high-silica CHA zeolite containing encapsulated Pt species by combining the use of TMAdA and Pt-mercapto complexes as OSDA and Pt-precursors, respectively. Most importantly, it has been shown that, by controlling the activation treatment, it is possible to prepare materials in where the nature and architecture of the Pt species can be tuned reversibly, from isolated atoms to nanometric particles.

ASSOCIATED CONTENT

(Word Style "TE_Supporting_Information"). **Supporting Information**. A brief statement in nonsentence format listing the contents of material supplied as Supporting Information should be included, ending with "This material is available free of charge via the Internet at http://pubs.acs.org." For instructions on what should be included in the Supporting Information as well as how to prepare this material for publication, refer to the journal's Instructions for Authors.

AUTHOR INFORMATION

Corresponding Author

* Corresponding author: E-mail addresses: acorma@itq.upv.es, pedro.m.serna-merino@exxonmobil.com

ACKNOWLEDGMENT

This work has been supported by the European Union through the SYNCATMATCH project (Grant Agreement nº 671093), and the Spanish Government through "Severo Ochoa Program" (SEV 2012-0267), and MAT2015-71261-R. This research used beamline 9-BM of the Advanced Photon Source, a U.S. Department of Energy (DOE) Office of Science User Facility operated for the DOE Office of Science by Argonne National Laboratory under Contract No. DE-AC02-06CH11357. The Electron Microscopy Service of the UPV is acknowledged for their help in sample characterization. We thank Isabel Millet and Paul Stevens for technical assistance, and Randall Meyer and Aaron Sattler for review of the manuscript. We appreciate the support of ExxonMobil Research and Engineering for our efforts in fundamental catalytic research.

REFERENCES

(1) Climent, M. J.; Corma, A.; Iborra, S. *Chem. Rev.*, **2011**, *111*, 1072-1133.
(2) Corma, A.; García, H. *Topics Catal.*, **2008**, *48*, 8-31.
(3) Haruta, M. Chem. Rec., **2003**, *3*, 75-87.
(4) Oliver-Meseguer, J.; Cabrero-Antonino, J. R.; Domínguez, I.; Leyva-Pérez, A; Corma, A. *Science*, **2012**, *338*, 1452-1455.
(5) Hunt, S. T.; Milina, M.; Alba-Rubio, A. C.; Hendon, C. H.; Dumesic, J. A.; Román-Leshkov, Y. *Science*, **2016**, *352*, 974-978.
(6) Tang, H.; Wei, J.; Liu, F.; Qiao, B.; Pan, X.; Li, L.; Liu, J.; Wang, J.; Zhang, T. *J. Am. Chem. Soc.*, **2016**, *138*, 56-59.
(7) Canlas, C. P.; Lu, J.; Ray, N. A.; Grosso-Giordano, N. A.; Lee, S.; Elam, J. W.; Winans, R. E.; Van Duyne, R. P.; Stair, P. C.; Notestein, J. M. *Nature Chem.*, **2012**, *4*, 1030-1036.
(8) Lu, J.; Fu, B.; Kung, M. C.; Xiao, G.; Elam, J. W.; Kung, H. H.; Stair, P. C. *Science*, **2012**, *335*, 1205-1208.
(9) Wang, G. H.; Hilgert, J.; Richter, F. H.; Wang, F.; Bongard, H. J.; Spliethoff, B.; Weidenthaler, C.; Schüth, F. *Nature Mater.*, **2014**, *13*, 293-300.
(10) Schatler, W. M. *Acc. Chem. Res.*, **1993**, *26*, 383-387.
(11) Ryoo, R.; Cho, S. J.; Pak, C.; Kim, J. G.; Ihm, S. K.; Lee, J. Y. *J. Am. Chem. Soc.*, **1992**, *114*, 76-82.
(12) Guczi, L.; Kiricsi, I. *Appl. Catal. A*, **1999**, *186*, 375-394.
(13) Creyghton, E. J.; van Duin, A. C. T.; Jansen, J. C.; Kooyman, P. J.; Zandbergen, H. W.; van Bekkum, H. *J. Chem. Soc., Faraday Trans.*, **1996**, *92*, 4637-4642.
(14) Yang, H.; Chen, H.; Chen, J.; Omotoso, O.; Ring, Z. *J. Catal.*, **2006**, *243*, 36-42.
(15) Moliner, M.; Martínez, C.; Corma, A. *Chem. Mater.*, **2014**, *26*, 246-258.
(16) Zhan, B.; Iglesia, E. *Angew. Chem. Int. Ed.*, **2007**, *46*, 3697-3700.
(17) Choi, M.; Wu, Z.; Iglesia, E. *J. Am. Chem. Soc.*, **2010**, *132*, 9129-9137.
(18) Altwasswe, S.; Gläser, R.; Weitkamp, J. *Micropor. Mesopor. Mater.*, **2007**, *104*, 281-288.
(19) Yang, H.; Chen, H.; Du, H.; Hawkins, R.; Craig, F.; Ring, Z.; Omotoso, O.; Munoz, V.; Mikula, R. *Micropor. Mesopor. Mater.*, **2009**, *117*, 33-40.
(20) Im, J.; Shin, H.; Jang, H.; Kim, H.; Choi, M. *Nat. Commun.*, **2014**, 5:3370.
(21) Wu, Z.; Goel, S.; Choi, M.; Iglesia, E. *J. Catal.*, **2014**, *311*, 458-468.
(22) Lee, S.; Lee, K.; Im, J.; Kim, H.; Choi, M. *J. Catal.*, **2015**, *325*, 26-34.

(23) Chen, H.; Yang, H.; Omotoso, O.; Ding, L.; Briker, Y.; Zheng, Y.; Ring, Z. *Appl. Catal. A*, **2009**, *358*, 103-109.
(24) Joel, S.; Wu, Z.; Zones, S. I.; Iglesia, E. *J. Am. Chem. Soc.*, **2010**, *134*, 17688-17695.
(25) Moliner, M.; Rey, F.; Corma, A. *Angew. Chem. Int. Ed.*, **2013**, 52, 13880-13889.
(26) Budroni, G.; Corma, A. *Angew. Chem. Int. Ed.*, **2006**, *45*, 3328-3331.
(27) Zones, S. I., *U.S. Patent 4544538*, **1985**.
(28) Zones, S. I.; Hwang, S. J. *Micropor. Mesopor. Mater.*, **2011**, *146*, 48-56.
(29) Ashtekar, S.; Chilukuri, S. V. V.; Chakrabarty, D. K. *J. Phys. Chem.*, **1998**, *98*, 4878-4883.
(30) Zones, S. I.; Yuen, L.; Miller, S. J. *U.S. Patent 6709644*, **2004**.
(31) Martinez-Franco, R.; Moliner, M.; Thogersen, J. R.; Corma, A. *ChemCatChem*, **2013**, 5, 3316-3323.
(32) Sun, Q.; Wang, N.; Guoa, G.; Yu, J. *Chem. Commun.*, **2015**, *51*, 16397-16400.
(33) Xu, T.; Helton, T. E.; Dakka, J. M.; Chen, T. J.; Miseo, S.; Decaul, L. C.; Lemon, E. A., *WO2011/096999*, **2011**.
(34) Ravel, B.; Newville, M. *J. Synchrotron Radiat.*, **2005**, *12*, 537-541.
(35) Zabinsky, S. I.; Rehr, J. J.; Ankudinov, A.; Albers, R. C.; Eller, M. J. *Phys. Rev. B*, **1995**, 52, 2995-3009.
(36) Martin, N.; Moliner, M., Corma, A. *Chem. Commun.*, **2015**, *51*, 9965-9968.
(37) Iler, R. K. The Chemistry of Silica: Solubility, Polymerization, Colloid and Surface Properties and Biochemistry of Silica. Wiley (**1979**).
(38) Kistler, J. D.; Chotigkrai, N.; Xu, P.; Enderle, B.; Praserthdam, P.; Chen, C. Y.; Browning, N. D.; Gates, B. C. *Angew. Chem. Int. Ed.*, **2014**, 53, 8904-8907.
(39) Wang, Q.; Hanson, J. C.; Frenkel, A. I. *J. Chem. Phys.*, **2008**, *129*, 234502-234507.
(40) de Graaf, J.; van Dillen, A. J.; de Jong, K. P.; Koningsberger, D. C. *J. Catal.*, **2001**, *203*, 307-321.
(41) Uzun, A.; Gates, B. C. *Angew. Chem. Int. Ed.*, **2008**, *47*, 9245–9248.
(42) Serna, P.; Gates, B. C. *J. Am. Chem. Soc.*, **2011**, *133*, 4714-4717.
(43) Treacy, M. M. J. *Micropor. Mesopor. Mater.*, **1999**, *28*, 271-292.
(44) Kulkarni, A.; Lobo-Lapidus, R. J.; Gates, B. C. *Chem. Commun.*, **2010**, *46*, 5997-6015.
(45) Hedin, N.; DeMartin, G. J.; Roth, W. J.; Strohmaier, K. G.; Reyes, S. C. *Micropor. Mesopor. Mater.*, **2008**, *109*, 327-334.

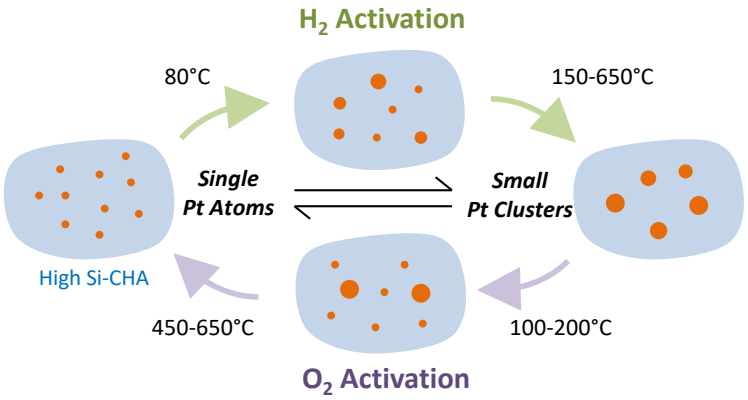
H2 Activation
80°C
150-650°C
Single
Pt Atoms
Small
Pt Clusters
High Si-CHA
450-650°C
100-200°C
O2 Activation